JOURNAL OF THERMOPHYSICS AND HEAT TRANSFER
Vol. 14, No. 1, January–March 2000

Accurate Determination of View Factors in Axisymmetric Enclosures with Shadowing Bodies Inside

Subrahmanya S. Katte* and S. P. Venkateshan†
Indian Institute of Technology, Chennai 600 036, India

A method is presented for calculating view factors accurately in a general enclosure with shadowing objects present inside, in which the surfaces are either axisymmetric bodies of revolution or planar, which has application in the thermal analysis of spacecraft systems. The view factor from an infinitesimally small ring element to a small band on the enclosure is evaluated by application of the contour integration method accounting for the shadowing effect, followed by numerical integration over finite lengths and decomposition rule. The solution of many practical thermal radiation problems in enclosures requires the knowledge of the view factors for a conical enclosure inside which a coaxial cylinder is present. An analytical expression for the view factor from an infinitesimally small ring element on the cone to the end disk is presented. The view factors from the lateral surface of the cone to the end disk are presented in graphical form for a representative case, which is not available in the literature. The preceding technique is applied to a sample enclosure to bring out the shadowing effect, and the results show an accuracy of up to six significant digits in the computed view factors.

Nomenclature

A, B, C, D, E	= surfaces comprising the enclosure
A_1, A_2	= ring elements having finite lengths on the enclosure, m^2; lateral surface and end disk for the conical enclosure, m^2
C_l, C_m, C_n	= contour integrals over dA_2 [Eq. (1)]
dA_1	= infinitesimally small element on A_1, m^2
dA_2	= infinitesimally small ring element on A_2, m^2
e	= point on the top of the inside cylinder as in Fig. 2a
F	= diffuse view factor
L, L_1, L_2, L_3	= dimensions of the enclosure, m
l_1, m_1, n_1	= direction cosines of dA_1
N_R	= nondimensional end disk radius of the conical enclosure (Fig. 4)
N_r	= dimensionless coordinate, r/R_1
p-p'	= line on the inside cylinder along which the rays from dA_1 are tangential (Fig. 2a)
$\mathfrak{R}$	= dimensionless distance between locations (X_1, Y_1, Z_1) and (X_2, Y_2, Z_2) [Eq. (2b)]
R_1	= inside cylinder radius, m (Fig. 1)
R_2, R_3	= radii of the enclosure, m
r	= radial coordinate, m
S-S'	= line on the enclosure that corresponds to the shadow of line p-p' (Fig. 2a)
X, Y, Z	= dimensionless Cartesian coordinates, x/R_1, y/R_1, z/R_1
x, y, z	= Cartesian coordinates, m
α_p	= angle defined in Fig. 2c, rad
β	= cone angle, radians
θ	= angular coordinate measured from x axis, rad
ξ	= dimensionless distance, z/R_1
ξ_1	= nondimensional distance of dA_1 from left end of inside cylinder (Fig. 2a)
ξ_2, ξ_3	= nondimensional distances of dA_2 from dA_1 (Fig. 2a)
ϕ	= angular coordinate measured from y axis, rad
ϕ_i, ϕ_m	= angles defined in Fig. 4, rad

Subscripts

c, d, e, f	= points c, d, e, and f, respectively, on the contour of dA_2 (Fig. 3)
E	= enclosure
l	= local
max	= maximum
p	= any point p on the inside cylinder
S	= point S, which is the shadow of point p
0, 1, 2	= points 0, 1, and 2, respectively, used for interpolation [Eq. (4)]
1, 2	= elements dA_1 and dA_2, respectively
$\parallel$	= parallel

Introduction

FOR spacecraft the primary mode of heat transfer in many instances between internal surfaces is thermal radiation. Because of the geometrical complexity of a spacecraft, the analytical determination of the net heat-exchange rates between surfaces is mathematically very difficult. To make mathematical analysis of radiant heat exchange feasible, the spacecraft is modeled into units like cylinders, frustum of cones, spheres and so on, and each unit is analyzed, assuming its surface to be isothermal. The enclosure is divided into a number of discrete isothermal segments, referred to as nodes. The thermal behavior of the system is described by the thermal capacities and conductive and radiative couplings that form the analytical model.[1] How well this model represents the actual system is determined largely by how isothermal the assigned nodes are. For pure radiation problems a detailed temperature distribution may not be needed, and an enclosure may be divided into a relatively few thermal nodes. With conduction and convection present in the system, there is a need for finer detail, and, hence, the system has to be divided into a relatively large number of nodes.

Because of the shielding action of objects in the interior, different locations on the spacecraft enclosure interact to varying degrees with other locations of the enclosure. In other words, an observer stationed at one element on the enclosure will see varying amounts of the neighboring elements as he changes his location. In addition, the extent of the interior part surface area that interacts with the

Received 19 February 1999; revision received 24 August 1999; accepted for publication 10 September 1999.

*Research Scholar, Madras; also Lecturer in Mechanical Engineering, Shanmugha College of Engineering, Tirumalaisamudram 613 402, India.

†Professor, Heat Transfer and Thermal Power Laboratory, Department of Mechanical Engineering, Madras; spv35@hotmail.com.

enclosure is also a function of the particular surface location on the enclosure. The major obstacle in the thermal analysis of such an enclosure with a shadowing object inside is the determination of view factors between the surface elements of the enclosure including shadowing effect. Without a method to evaluate view factors accurately, meaningful analysis is impossible, and hence emphasis has been given for the accurate determination of view factors.[2] It would be ideal if analytical solutions existed for view factors between any pair of diffuse surfaces. This, however, is not so except for a few simple configurations, which are listed in a number of references. A typical compilation of view factors[3] shows the following:

View factor expressions are available for cylindrical and conical enclosures separately in the literature[4–6] without any shadowing bodies inside. An enclosure of two concentric cylinders has also been considered[7–9] but having identical finite lengths. Sparrow et al.[10] obtained view factors for an annular-finned space radiator including the shielding action of the tube by applying the contour integration method. There have been applications of the contour integration method for the evaluation of view factors including shielding action of the base surface for the optimization of tubular space radiator.[11,12] Meng and Zhang[13] proposed a technique for the calculation of view factors between many bodies in an irregularly shaped chamber, but with a maximum deviation of about 2% from the sum rule, which is not satisfactory.

From a survey of the available literature, there has been no attempt for the accurate and efficient determination of view factors in a general enclosure, inside which shadowing objects are present, when all of the bodies are axisymmetric bodies of revolution. The motivation for the present study was indeed a desire to indicate a method to determine view factors accurately and efficiently in such an enclosure, accounting for the shadowing effect of internals, by the application of the contour integration method, followed by numerical integration.

For the purpose of this paper, we shall consider a general enclosure of the type shown in Fig. 1. The enclosure is made up of a cylinder and frustum of a cone with another smaller cylinder of arbitrary length inside, which is the shadowing object. All of the three geometries are axisymmetric. In the following work all of the dimensions are normalized with respect to R_1, the radius of the inside cylinder. View factors between elements on the enclosure, including shadowing action of the inside cylinder are obtained by the application of contour integration method, followed by numerical integration over finite lengths and decomposition rule. However, the view factors from the inside cylinder to all other elements on the enclosure can be obtained by expressions available in the literature and view factor algebra. To obtain the view factor F_{A_1,A_2}, when finite length area elements A_1 and A_2 are located anywhere on the enclosure, first an infinitesimally small element dA_1 (having a length of $dz/\cos\beta$ and a width of $N_{r,l}d\theta$) on A_1 and a small band dA_2 on A_2 are considered. From the rule for a subdivided emitting area, F_{dA_1,dA_2} is equivalent to the view factor from an infinitesimally small ring element dA_1 ring to dA_2. From dA_1, rays are generated in all directions bounding the contour of the shadowing object and are extended to meet the enclosure, thus evaluating the shape and size of the shadow on the enclosure. Once coordinates of all points on the shadow are calculated, F_{dA_1,dA_2} is evaluated by the application of the contour integration method, which is outlined in what follows. F_{dA_1,dA_2} is then numerically integrated twice, once each over the lengths of elements A_1 and A_2. By adapting suitable step sizes for these integration, the view factors can be evaluated accurately up to six significant digits, with a maximum deviation of 2×10^{-6} % from the sum rule, when all of the view factors in the enclosure are independently calculated.

Analysis

View Factors Between Enclosure Elements by Contour Integration

To demonstrate the fact that the results not already available in the literature can be derived from the contour integral representation, let us consider the interchange between an infinitesimally small element dA_1 and a small band dA_2 on the enclosure (Fig. 2a). For the sake of generality, dA_1 is located on conical portion at a nondimensional distance of ξ_1 from the left end of the inner cylinder and dA_2 on the cylindrical portion of the enclosure. It is convenient to orient the coordinate axes so that a component of normal or the normal to dA_1 lies precisely along a coordinate line. Then, at least one or at most two of the three direction cosines of dA_1 are zero, and a large portion of the contour integral vanishes, as will be seen later.

As seen from dA_1, the inside cylinder casts a shadow on the enclosure in regions I and II only, and beyond region II there will not be any shadow. The regimes of the shadow regions I and II are found by constructing a tangent to the inside cylinder from dA_1 to pass through point p and joining the top edge of the inside cylinder (point e) and dA_1. Figure 2a shows that the energy leaving dA_1 and tangent to the inside cylinder along the line p-p' will leave a shadow on the horizontal line S-S'. The shadow line S-S' is parallel to the z axis up to a distance of $\xi_{S,\|} = \xi_1[\sqrt{(N_{r,E}^2 - 1)} + \sqrt{(N_{r,l}^2 - 1)}]/\sqrt{(N_{r,l}^2 - 1)}$, if the shadow falls on the cylindrical portion of the enclosure. This defines region I. Region II is where the inner cylinder casts a shadow on the enclosure that is no longer parallel to the z axis because the energy is now tangent to the end of the cylinder along p-e. Point $S_{\max}$, which corresponds to the point e, marks the boundary beyond which there is no shadow, which is region III. Regions I and II stretch from dA_1 to a maximum distance of $\xi_{S,\max} = (N_{r,E} + N_{r,l})\xi_1/(N_{r,l} - 1)$. The expressions for $\xi_{S,\|}$ and $\xi_{S,\max}$ can be obtained from similar triangles in Figs. 2a–2c. The details of the derivation are given later, for a general point p.

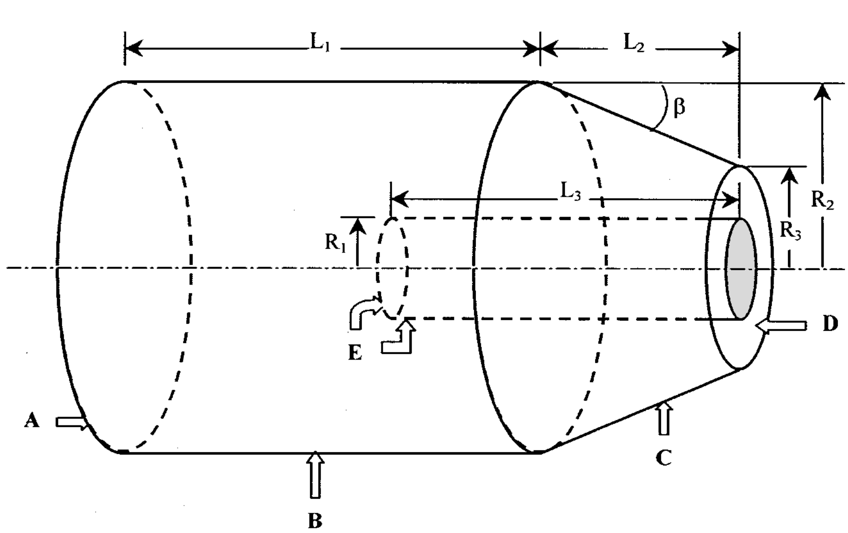

Fig. 1 General axisymmetric enclosure considered in the present study.

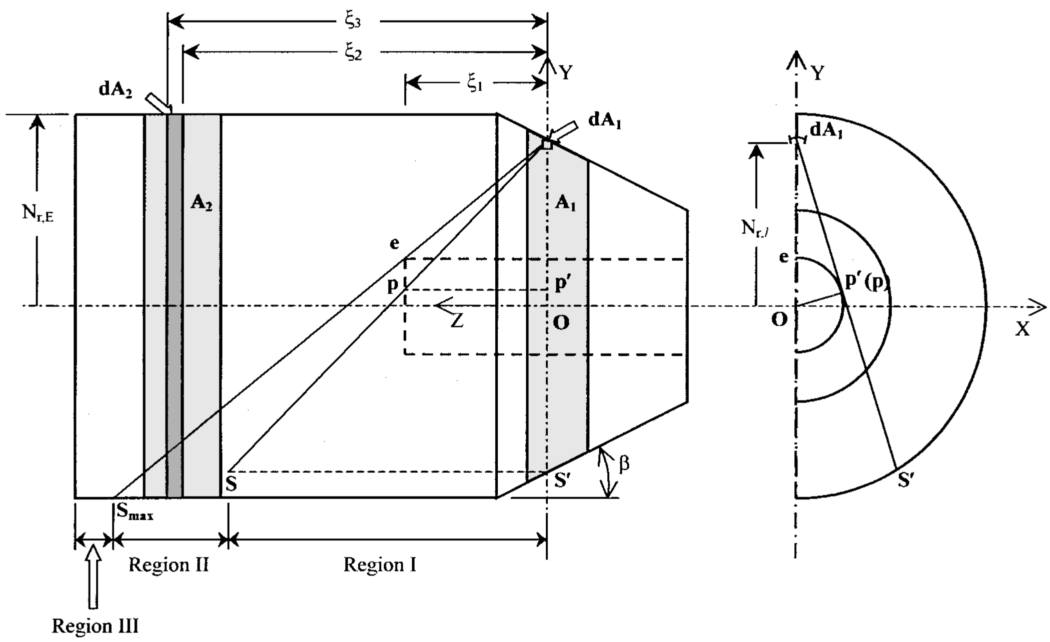

Fig. 2a Locations of area elements for view factor determination.

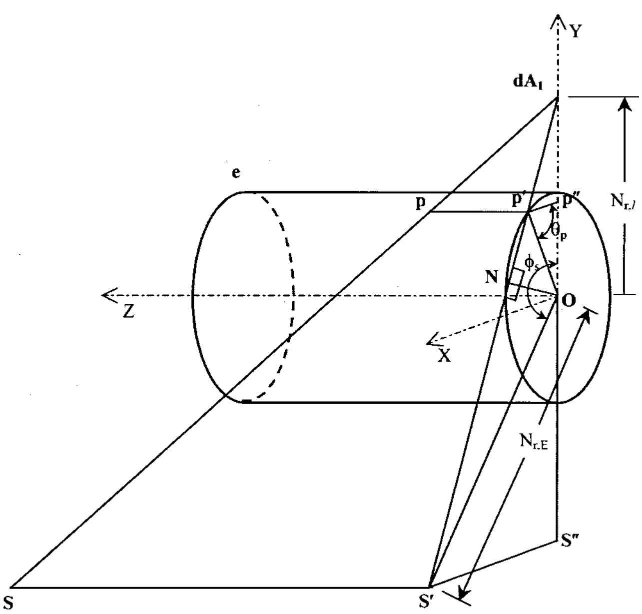

Fig. 2b Coordinates of area elements: pictorial front view.

Because of the shielding action of the inner cylinder, radiant energy from a typical element dA_1 is able to strike only a portion of the band dA_2 if it is located in region I or II. Further, the limits of visibility depend on the location of the band dA_2 in the enclosure. The portion of the band dA_2 that exchanges radiation with dA_1 is found by constructing lines from dA_1 that are tangent to the inside cylinder and by extending them to meet the band dA_2. As shown in Fig. 3, the element dA_2 is not a complete band; rather the arcs are truncated by the tangent lines already discussed. Clearly, the angular span of the band A_2 remains constant in region I with line c-d parallel to the z axis if the enclosure is cylindrical and varies otherwise or increases in region II as we move in positive z direction. If dA_2 is located in region III, there is no shielding effect of the inside cylinder at all, and it is a complete band. For this case expressions for the view factors are already available in the literature.[7] When the band dA_2 is located in region I or II, obtaining the view factor F_{dA_1,dA_2} is a challenging problem because of the nonelementary shape of dA_2 and also because part of dA_2 visible from dA_1 changes shape and size depending on its location on the enclosure. The customary approach to determining angle factors is to attempt to evaluate integrals over the participating surface areas. However, this can be a formidable task even for simple situations. In the present work, the area integrals are replaced by contour integrals using the method introduced by Sparrow,[14] which has been used by many authors to account for the shadowing effect while evaluating view factors.[10–12] This analysis will be carried out first for the angle factor F_{dA_1,dA_2}.

Following the analysis of Sparrow, the angle factor can be written as

$$F_{dA_1,dA_2} = l_1 C_l + m_1 C_m + n_1 C_n \tag{1}$$

Because the normal to dA_1 makes an angle of β with the y axis, then $l_1 = 0, m_1 = -\cos\beta, n_1 = \sin\beta$. With this the angle factor becomes

$$2\pi F_{dA_1,dA_2} = m_1 \oint_C \frac{(X_2 - X_1)\,\mathrm{d}Z_2 - (Z_2 - Z_1)\,\mathrm{d}X_2}{\Re^2} + n_1 \oint_C \frac{(Y_2 - Y_1)\,\mathrm{d}X_2 - (X_2 - X_1)\,\mathrm{d}Y_2}{\Re^2} \tag{2a}$$

in which the dimensionless distance $\Re$, between dA_1 and points on the boundary of A_2, is given by

$$\Re^2 = (X_2 - X_1)^2 + (Y_2 - Y_1)^2 + (Z_2 - Z_1)^2 \tag{2b}$$

The coordinates may be identified with the aid of Figs. 2a–2c. For the element dA_1, $X_1 = 0, Y_1 = N_{r,l}$, and $Z_1 = 0$. For dA_2, X_2, Y_2, and Z_2 vary around the contour. To find the limits of visibility of dA_2, points c and d in Fig. 3, the following procedure is used. For any point p on the inside cylinder, dimensionless coordinates are given by $(\cos\theta_P, \sin\theta_P, \xi_P)$. By drawing a line from dA_1 through point p and extending it to meet the enclosure, we can get the coordinates of the point S on the shadow, which corresponds to point p as follows. As shown in Figs. 2b and 2c, the angle $\phi_S = \angle dA_1 ON + \angle NOS'$ is the angle between the y axis and the line connecting O and S'. The point N is chosen on the line between dA_1 and S' so as to form two right angles. This gives the limit of integration as

$$\phi_s = \cos^{-1}(ON/N_{r,l}) + \cos^{-1}(ON/N_{r,E}) \tag{3}$$

in which $ON = N_{r,l}\sin\alpha_p$ with $\alpha_p = \tan^{-1}[\cos\theta_P/(N_{r,l} - \sin\theta_P)]$. Now, X and Y coordinates of point S can be identified with the aid of Fig. 2c. The z value can be found using the two sets of similar triangles (dA_1-p-p' and dA_1-S-S') and (dA_1-p'-p'' and dA_1-S'-S''). Thus coordinates of point S are given by $[N_{r,E}\sin\phi_s, N_{r,E}\cos\phi_s, \xi_P(N_{r,l} - N_{r,E}\cos\phi_s)/(N_{r,l} - \sin\theta_p)]$.

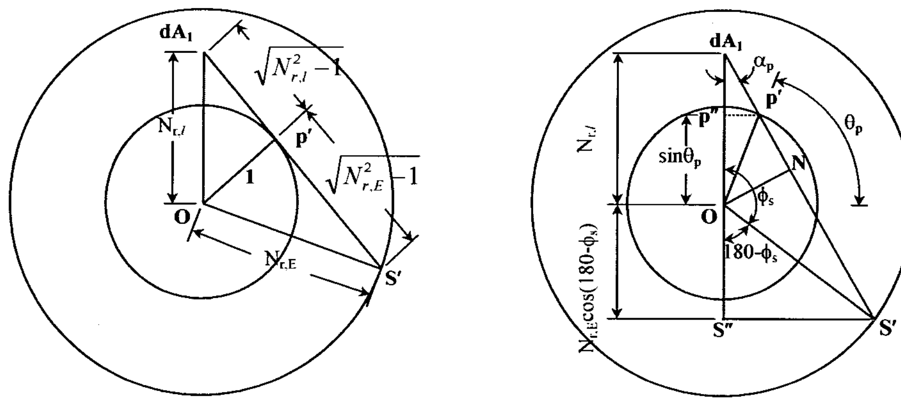

dA$_1$-p Tangent to Inner Cylinder
dA$_1$-p not Tangent to Inner Cylinder

Fig. 2c Coordinates of area elements: end view.

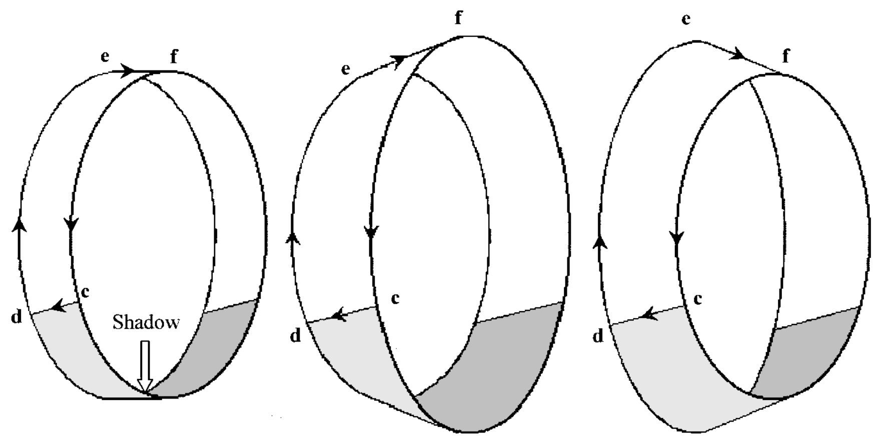

Fig. 3 Direction of contour integration for dA_2 and possible configurations of dA_1 or dA_2.

For dA_2 the minimum angle $\phi = \phi_m$ occurs when the line joining dA_1 and S is tangential to lateral surface of the inside cylinder, with $ON = 1$ in Eq. (3), and maximum angle $\phi = \pi$ occurs when dA_2 is located in region III, where there is no shadowing effect. Here ϕ covers only one side of the enclosure. Symmetry will be used to account for both sides. Now the arc p'-e on the cylinder end (Fig. 2a) is divided into a number of divisions, and coordinates of the points on the shadow on the enclosure, corresponding to each division, are obtained. The number of divisions to be made is found by a convergence test of view factors obtained. X and Y coordinates of points c and d on the band dA_2 are obtained by interpolation in region II, corresponding to Z coordinates that are given by ξ_2 and ξ_3, respectively, and segment c-d is treated as a discretized straight line in the band dA_2. However, if the band dA_2 is located in region I, c-d is a straight line for both cylindrical and conical enclosures and shadowing objects, with X and Y coordinates corresponding to the lines that are tangential to lateral surface of the shadowing object. The interpolation in region II, in order to obtain coordinates of c and d, is done by fitting the second-order Lagrange interpolating polynomial to the Y coordinates obtained. Indeed, the shadow on the enclosure in region II is a second-order space curve. The Y coordinate corresponding to any Z coordinate, which is known, is given by

$$Y_S = \frac{(Z - Z_1)(Z - Z_2)}{(Z_0 - Z_1)(Z_0 - Z_2)} Y_0 + \frac{(Z - Z_0)(Z - Z_2)}{(Z_1 - Z_0)(Z_1 - Z_2)} Y_1 + \frac{(Z - Z_0)(Z - Z_1)}{(Z_2 - Z_0)(Z_2 - Z_1)} Y_2 \tag{4}$$

in which coordinates of adjoining points 0, 1, and 2 are known, which corresponds to the coordinates of points obtained corresponding to the divisions on arc p'-e. However, the X coordinate corresponding to any Y coordinate is obtained by the equation of the enclosure at that particular location $X_S = \sqrt{(N_{r,E}^2 - Y_S^2)}$. Once the coordinates of the points c and d and limits of integration ϕ are identified by the procedure just outlined, it is convenient to subdivide the contour of dA_2 into several segments. The direction of travel along the contour for integration is shown in Fig. 3. This is determined by requiring that an observer, walking along the contour with his body aligned with the normal, keeps the interior of the area dA_2, at his left.

Considering first the arc f-c, it is convenient to introduce polar coordinates $X_2 = N_{r,E} \sin\phi$, $Y_2 = N_{r,E} \cos\phi$, and $Z_2 = \xi_2$ remains constant. With these, $\mathrm{d}X_2 = N_{r,E} \cos\phi \, \mathrm{d}\phi$, $\mathrm{d}Y_2 = -N_{r,E} \sin\phi \, \mathrm{d}\phi$, and $\Re^2 = N_{r,I}^2 + N_{r,E}^2 + \xi_2^2 - 2N_{r,I}N_{r,E}\cos\phi$. Substituting into Eq. (2), the integral over f-c becomes

$$2\pi F_{dA_1,dA_{2,f\text{-}c}} = m_1 \int_0^{\phi_C} \frac{-\xi_2 N_{r,E} \cos\phi \, \mathrm{d}\phi}{N_{r,I}^2 + N_{r,E}^2 + \xi_2^2 - 2N_{r,I}N_{r,E}\cos\phi} + n_1 \int_0^{\phi_C} \frac{N_{r,E}^2 - N_{r,I}N_{r,E}\cos\phi}{N_{r,I}^2 + N_{r,E}^2 + \xi_2^2 - 2N_{r,I}N_{r,E}\cos\phi} \, \mathrm{d}\phi \tag{5a}$$

The integration can be carried out to obtain the following result in closed form:

$$2\pi F_{dA_1,dA_{2,f\text{-}c}} = \frac{\phi_C}{2}\left(\frac{m_1\xi_2}{N_{r,I}} + n_1\right) + \frac{1}{\sqrt{a_2^2 - b^2}} \tan^{-1}\left[\frac{\tan(\phi_C/2)}{\sqrt{(a_2 - b)/(a_2 + b)}}\right] \times \left[n_1(N_{r,E}^2 - N_{r,I}^2 - \xi_2^2) - \frac{m_1\xi_2 a_2}{N_{r,I}}\right] \tag{5b}$$

The contour integral over arc d-e can be carried out in a manner similar to that employed for the arc f-c, with the result

$$2\pi F_{dA_1,dA_{2,d-e}} = \frac{\phi_d}{2}\left(-n_1 - \frac{\xi_3 m_1}{N_{r,l}}\right) + \frac{1}{\sqrt{a_3^2 - b^2}}\tan^{-1}\left[\frac{\tan(\phi_d/2)}{\sqrt{(a_3-b)/(a_3+b)}}\right] \times \left[\frac{m_1\xi_3 a_3}{N_{r,l}} - n_1(N_{r,E}^2 - N_{r,l}^2 - \xi_3^2)\right]$$

in which

$$a_2 = N_{r,E}^2 + N_{r,l}^2 + \xi_2^2, \qquad a_3 = N_{r,E}^2 + N_{r,l}^2 + \xi_3^2$$
$$b = 2N_{r,l}N_{r,E} \tag{6}$$

Considering the integrals over discretized straight-line segment c-d, the equation of this line is

$$\frac{X_2 - X_c}{X_d - X_c} = \frac{Y_2 - Y_c}{Y_d - Y_c} = \frac{Z_2 - Z_c}{Z_d - Z_c}$$

From this,

$$\mathrm{d}X_2 = \frac{(X_d - X_c)}{(Z_d - Z_c)}\,\mathrm{d}Z_2 = \frac{(X_d - X_c)}{(Y_d - Y_c)}\,\mathrm{d}Y_2$$

With these, the integrals over line c-d, Eq. (2a), become

$$2\pi F_{dA_1,dA_{2,c-d}} = m_1(Z_d - Z_c)(X_cZ_d - X_dZ_c) \times \int_{Z_2=\xi_2}^{\xi_3} \frac{\mathrm{d}Z_2}{a_4 + b_4Z_2 + cZ_2^2} + n_1(Y_d - Y_c)[N_{r,l}(X_c - X_d) + (X_dY_c - X_cY_d)]\int_{Y_2=Y_c}^{Y_d}\frac{\mathrm{d}Y_2}{a_5 + b_5Y_2 + cY_2^2}$$

in which

$$a_4 = (X_cZ_d - X_dZ_c)^2 + [Y_cZ_d - Y_dZ_c - N_{r,l}(Z_d - Z_c)]^2$$
$$b_4 = 2(X_d - X_c)(X_cZ_d - X_dZ_c) + 2(Y_d - Y_c)[Y_cZ_d - Y_dZ_c - N_{r,l}(Z_d - Z_c)]$$
$$c = (X_d - X_c)^2 + (Y_d - Y_c)^2 + (Z_d - Z_c)^2$$
$$a_5 = (X_cY_d - X_dY_c)^2 + (Y_dZ_c - Y_cZ_d)^2 + N_{r,l}^2(Y_d - Y_c)^2$$
$$b_5 = 2(X_d - X_c)(X_cY_d - X_dY_c) - 2N_{r,l}(Y_d - Y_c)^2 + 2(Z_d - Z_c)(Y_dZ_c - Y_cZ_d) \tag{7}$$

The integration can be carried out to obtain the following result in closed form:

$$2\pi F_{dA_1,dA_{2,c-d}} = m_1(Z_d - Z_c)(X_cZ_d - X_dZ_c)\frac{2}{\sqrt{q_4}} \times \left[\tan^{-1}\left(\frac{2c\xi_3 + b_4}{\sqrt{q_4}}\right) - \tan^{-1}\left(\frac{2c\xi_2 + b_4}{\sqrt{q_4}}\right)\right] + n_1(Y_d - Y_c)[N_{r,l}(X_c - X_d) + (X_dY_c - X_cY_d)]\frac{2}{\sqrt{q_5}} \times \left[\tan^{-1}\left(\frac{2cY_d + b_5}{\sqrt{q_5}}\right) - \tan^{-1}\left(\frac{2cY_c + b_5}{\sqrt{q_5}}\right)\right] \tag{8}$$

in which $q_4 = 4a_4c - b_4^2$ and $q_5 = 4a_5c - b_5^2$. If the line c-d is parallel to the z axis, the second term on the right-hand side of Eq. (8) vanishes.

On the straight-line e-f, $X_1 = X_2 = 0$; hence, both integrals in Eq. (2a) vanish identically.

Finally angle factor F_{dA_1,dA_2} may be obtained by noting the symmetry of the integral as

$$F_{dA_1,dA_2} = 2(F_{dA_1,dA_{2,f-c}} + F_{dA_1,dA_{2,c-d}} + F_{dA_1,dA_{2,d-e}}) \tag{9}$$

The preceding equation can be applied to both conical and cylindrical configurations of dA_1 and dA_2. If dA_1 lies on cylindrical portion of the enclosure, then $l_1 = 0$, $m_1 = -1$, and $n_1 = 0$, thereby a large portion of the contour integrals in the Eqs. (5b), (6), and (8) vanish.

Conical Enclosure with a Coaxial Cylinder Inside

The purpose of this section is to provide information, otherwise unavailable in the literature, on the view factor from lateral surface of the cone to end disk in a conical enclosure inside which a coaxial cylinder is present. An analytical expression is presented here for the view factor from an infinitesimally small ring element dA_1 on the cone to the end disk A_2. F_{dA_1,A_2} thus obtained is integrated numerically over the lateral surface of the cone to obtain the view factor from the lateral surface to the end disk F_{A_1,A_2}.

Let us consider radiant interchange between an infinitesimally small ring element dA_1 on the lateral surface A_1 of the cone at a nondimensional distance of ξ, and the end disk A_2 as pictured in Fig. 4. Because of the shielding action of the inside cylinder, radiant energy from a typical element dA_1 is able to strike only a portion of the A_2. The portion of the end disk that exchanges radiation with dA_1 is found by constructing lines from dA_1 that are tangent to the inside cylinder surface. As shown in Fig. 4, the portion of the end disk that receives radiation is not a complete disk, but rather the tangent line limits the radiation from dA_1 to contour a-b-c-d-a. Clearly, the angular span of the disk A_2 decreases as ξ increases and is a function of cone angle β. Finding the angle factor F_{dA_1,A_2} is a challenging problem because of the nonelementary shape of A_2 and also because A_2 changes size as ξ varies; hence, the area integrals are replaced by contour integrals. The required coordinates may be identified with the aid of Fig. 4. For the element dA_1, $X_1 = 0$, $Y_1 = N_{r,l}$, and $Z_1 = 0$. For A_2, X_2 and Y_2 vary around the contour, while $Z_2 = \xi$ remains constant. The direction of the integration around the contour is as shown in the diagram. With these, Eq. (2a) becomes

$$2\pi F_{dA_1,A_2} = m_1\oint_C \frac{-\xi\,\mathrm{d}X_2}{X_2^2 + (Y_2 - N_{r,l})^2 + \xi^2} + n_1\oint_C \frac{(Y_2 - N_{r,l})\,\mathrm{d}X_2 - X_2\,\mathrm{d}Y_2}{X_2^2 + (Y_2 - N_{r,l})^2 + \xi^2} \tag{10}$$

where the contour is a-b-c-d-a. It is convenient to subdivide the contour into several segments.

Consider first the integral over the straight line a-b. On line a-b, $X_2 = 0$ so that both integrals in Eq. (10) vanish identically. Considering the arc b-c, it is convenient to introduce polar coordinates $X_2 = N_R\sin\phi$ and $Y_2 = N_R\cos\phi$. With these, $\mathrm{d}X_2 = N_R\cos\phi\,\mathrm{d}\phi$, $\mathrm{d}Y_2 = -N_R\sin\phi\,\mathrm{d}\phi$, and $\Re^2 = N_R^2 + Nr_l^2 + \xi^2 - 2Nr_lN_R\cos\phi$. Substituting into Eq. (10), the integrals over b-c become

$$2\pi F_{dA_1,A_{2,b-c}} = m_1\int_0^{\phi_m}\frac{-\xi N_R\cos\phi\,\mathrm{d}\phi}{N_R^2 + N_{r,l}^2 + \xi^2 - 2N_RN_{r,l}\cos\phi} + n_1\int_0^{\phi_m}\frac{N_R^2 - N_{r,l}N_R\cos\phi}{N_R^2 + N_{r,l}^2 + \xi^2 - 2N_RN_{r,l}\cos\phi}\,\mathrm{d}\phi$$

in which the limit of integration

$$\phi_m = \cos^{-1}(1/N_{r,l}) + \cos^{-1}(1/N_R) \tag{11a}$$

The integration can be carried out to obtain the following result in closed form:

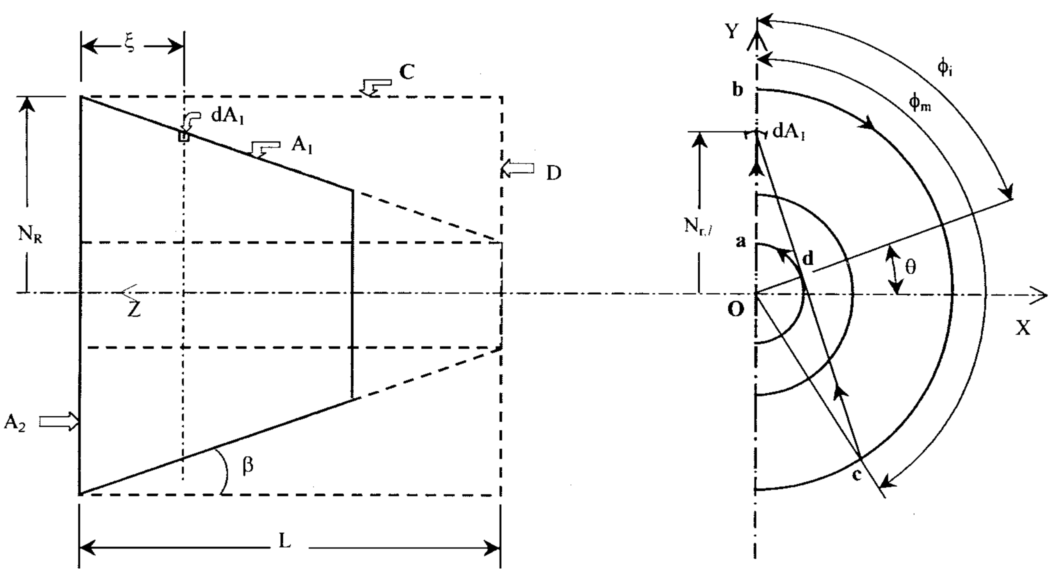

Fig. 4 Conical enclosure with a coaxial cylinder inside.

$$2\pi F_{dA_1,A_{2,b-c}} = \frac{\phi_m}{2}\left(\frac{m_1\xi}{N_{r,l}} + n_1\right) + \frac{1}{\sqrt{a_6^2 - b_6^2}}$$
$$\times \tan^{-1}\left[\frac{\tan(\phi_m/2)}{\sqrt{(a_6 - b_6)/(a_6 + b_6)}}\right]\left[n_1(2N_R^2 - a_6) - \frac{m_1\xi a_6}{N_{r,l}}\right] \tag{11b}$$

in which $a_6 = N_R^2 + N_{r,l}^2 + \xi^2$ and $b_6 = 2N_{r,l}N_R$.

Now consider the integral over the straight-line segment c-d. It is easily verified that the equation of this line is $Y_2 = N_{r,l} - \surd(N_{r,l}^2 - 1)X_2$. (The line passes through points $X = 0$, $Y = N_{r,l}$, and is tangent to the inner cylinder surface.) With this,

$$(Y_2 - N_{r,l})\,\mathrm{d}X_2 = -\sqrt{N_{r,l}^2 - 1}X_2\,\mathrm{d}X_2 = X_2\,\mathrm{d}Y_2$$

Therefore, the second term of Eq. (10) is identically zero on the segment c-d. Substituting the equation of line in Eq. (10), the integral over c-d becomes

$$2\pi F_{dA_1,A_{2,c-d}} = m_1\sqrt{N_{r,l}^2 - 1}\xi$$
$$\times \int_{Y_2 = N_R\cos\phi_m}^{\cos\phi_i} \frac{\mathrm{d}Y_2}{\left[\xi^2(N_{r,l}^2 - 1) + N_{r,l}^4\right] - 2N_{r,l}^3 Y_2 + N_{r,l}^2 Y_2^2} \tag{12a}$$

in which $\phi_i = \cos^{-1}(1/N_{r,l})$. The integration can be carried out to obtain the following result in closed form:

$$2\pi F_{dA_1,A_{2,c-d}} = \frac{m_1}{N_{r,l}}\left[\tan^{-1}\left(\frac{1 - N_{r,l}^2}{\xi\sqrt{N_{r,l}^2 - 1}}\right)\right.$$
$$\left. - \tan^{-1}\left(\frac{N_{r,l}N_R\cos\phi_m - N_{r,l}^2}{\xi\sqrt{N_{r,l}^2 - 1}}\right)\right] \tag{12b}$$

By a similar procedure, one can see that the integral over arc d-a becomes

$$2\pi F_{dA_1,A_{2,d-a}} = m_1\int_{\phi_i}^{0} \frac{-\xi\cos\phi\,\mathrm{d}\phi}{1 + N_{r,l}^2 + \xi^2 - 2N_{r,l}\cos\phi}$$
$$+ n_1\int_{\phi_i}^{0} \frac{(1 - N_{r,l}\cos\phi)\,\mathrm{d}\phi}{1 + N_{r,l}^2 + \xi^2 - 2N_{r,l}\cos\phi}$$

with the closed-form solution

$$2\pi F_{dA_1,A_{2,d-a}} = \frac{1}{\sqrt{a_7^2 - b_7^2}}\tan^{-1}\left[\frac{\tan(\phi_i/2)}{\sqrt{(a_7 - b_7)/(a_7 + b_7)}}\right]$$
$$\times \left[\frac{m_1\xi a_7}{N_{r,l}} + n_1(a_7 - 2)\right] - \frac{\phi_i}{2}\left(\frac{\xi m_1}{N_{r,l}} + n_1\right) \tag{13}$$

in which $a_7 = 1 + N_{r,l}^2 + \xi^2$ and $b_7 = 2N_{r,l}$.

A final expression for the view factor $F_{dA_1-A_2}$ may be obtained by taking advantage of symmetry as

$$F_{dA_1-A_2} = 2(F_{dA_1,A_{2,b-c}} + F_{dA_1,A_{2,c-d}} + F_{dA_1,A_{2,d-a}}) \tag{14}$$

Results and Discussion

The effect of shielding action of the inside cylinder on the view factors between elements on the enclosure is brought out now. The shadowing effect is studied first on F_{dA_1,dA_2} for a range of geometrical parameters and later on F_{A_1,A_2}.

View Factor F_{dA_1,dA_2}

F_{dA_1,dA_2} is plotted in Fig. 5 as a function of ξ, the distance of dA_2 from dA_1, when dA_1 is located on the cylindrical portion of the enclosure at a distance of $\xi_1 = 0.5$ from the left end of the inside cylinder. Element dA_2 with an axial width of 0.01 is located anywhere on the enclosure to the left of dA_1, and F_{dA_1,dA_2} is plotted against ξ for a wide range of radii ratios $N_{r,E}$ of the enclosure. Had the inside cylinder been of the same length as the outside cylinder (for which expressions are available in the literature[7,15]), F_{dA_1,dA_2} would have decreased monotonically when dA_2 is moved away from dA_1, as shown by curve A-F in Fig. 5, for an enclosure with $N_{r,E} = 2$. The effect of cutting off of the inside cylinder at a distance of ξ_1 from dA_1 (the view factor for such a configuration is not available in the literature) is to cause F_{dA_1,dA_2} to show a nonmonotonic behavior, even when dA_2 moves away from dA_1. This effect does not affect the view factor F_{dA_1,dA_2} until $\xi = \xi_{S,\|}$ ($0 < \xi < 1$ for the case considered—region I). In region I, F_{dA_1,dA_2} is the same as the case in which the inside cylinder is of the same length as the outside cylinder, as given by curve A-B. For $\xi_{S,\|} < \xi < \xi_{S,\max}$ ($1 < \xi < 2$ for the case considered—region II), as dA_2 moves away from dA_1, the shadow of the inside cylinder from dA_1 on dA_2 becomes smaller and smaller, thereby more and more surface area of dA_2 can see dA_1. But at the same time the view factor tends to decrease as dA_2 moves away from dA_1. In region II the uncovering effect of the shadow is dominant, and, hence, the net effect is an increase in F_{dA_1,dA_2} as

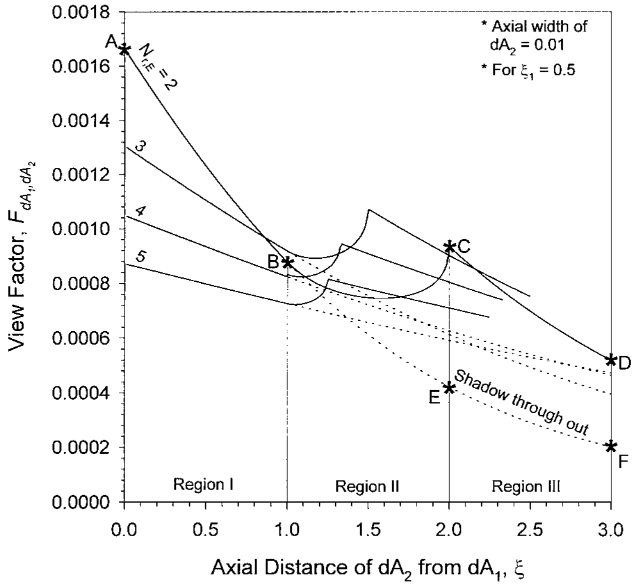

Fig. 5 Effect of shadowing on F_{dA_1,dA_2} when dA_1 and dA_2 are located on the cylindrical portion in Fig. 1.

shown by curve B-C. For $\xi > \xi_{S,\max}$ ($\xi > 2$ for the case considered—region III) there is no shadowing by the inside cylinder, and, hence, F_{dA_1,dA_2} monotonically decreases as dA_2 moves further away from dA_1 caused by the increasing distance as given by curve C-D. The uncovering effect of the shadow thus changes B-E-F to B-C-D in the present case.

For a given $N_{r,E}$ if ξ_1 is increased, or for a given ξ_1 if $N_{r,E}$ is reduced, then the range of the region II ($\xi_{S,\|} < \xi < \xi_{S,\max}$) increases. As the uncovering of the shadow takes place over a larger distance now, the change in F_{dA_1,dA_2} will be gradual with respect to ξ, when dA_2 moves away from dA_1.

View Factor F_{A_1,A_2}

To obtain the view factor F_{dA_1,A_2} (the view factor from dA_1 to a finite element A_2 on the enclosure), F_{dA_1,dA_2}, which is given by Eq. (9), has to be integrated over the axial width of A_2. Further, to obtain F_{A_1,A_2}, F_{dA_1,A_2} has to be again integrated over the length of A_1. Both integrations are done numerically. If A_2 is located in region II with respect to dA_1 or if the enclosure and shadowing objects are bodies of revolution other than cylinder and cones, then F_{dA_1,dA_2} is a strong function of location of dA_2 on the enclosure. This is especially so when dA_1 is located close to the left end of the inside cylinder or for large values of $N_{r,E}$. Hence for the numerical integration finite widths of elements A_1 and A_2 have to be divided into a relatively large number of small elements dA_1 and dA_2. The results improve with smaller grid sizes, but the computing time increases. Hence, optimum axial widths of dA_1 and dA_2 for the preceding integrations are determined by convergence tests.

As a critical case, view factors from dA_1 on the conical portion of the enclosure to all of region II on the cylindrical portion of the enclosure are compared, when region II is divided into a different number of small elements dA_2. The cone angle β considered here is 60 deg. Element dA_1 is located on the conical portion at a distance of $\xi_1 = 0.5$ from the left end of the inside cylinder for an enclosure with $N_{r,E} = 2$. Region II starts at an axial distance of 2.12 units and ends at an axial distance of 11.69 from dA_1. The percentage changes in the values of F_{dA_1,A_2} for two consecutive axial widths of dA_2 used for the numerical integration are plotted, as a function of axial width of dA_2 in Fig. 6. An axial width of dA_2 of ~0.03 is adequate for the integration of F_{dA_1,dA_2} over the length of A_2 to obtain F_{dA_1,A_2} with a change in the view factor of about 10^{-4} %.

Further, F_{dA_1,A_2} thus obtained is numerically integrated over the length of A_1 using Simpson's one-third rule to obtain F_{A_1,A_2}. Here both A_1 and A_2 are located on the cylindrical portion of the enclosure (with $N_{r,E} = 2$) with an axial width of 0.25 for both. A_2 is located at a mean distance of 2.25 from A_1, which lies in region II and which

Table 1 Comparison of results for limiting cases

		F_{A_1,A_2}	
N_R	β, deg	Present code	Ref. 15
	0	0.314998	0.314998
2	5	0.066367	0.066367
	80	0.932719	0.932719
	0	0.473768	0.473769
10	5	0.082013	0.082014
	80	0.970738	0.970739

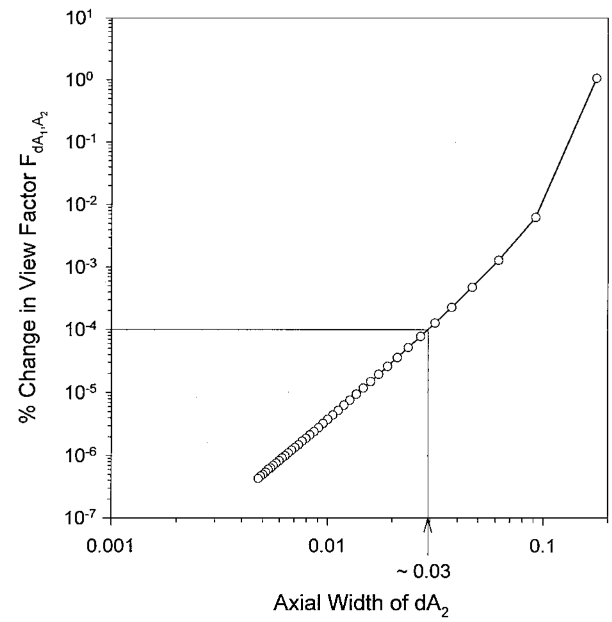

Fig. 6 Convergence study for choosing axial width of dA_2.

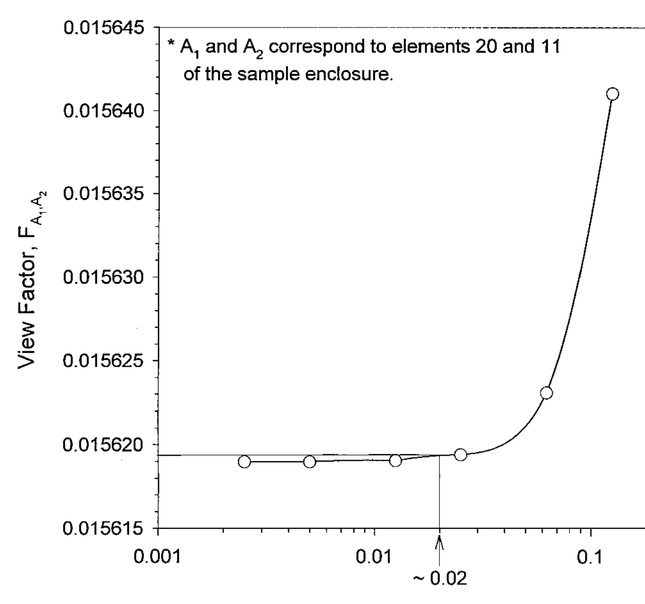

Fig. 7 Convergence study for choosing axial width of dA_1.

is a critical case (corresponds to elements 20 and 11 of sample enclosure). F_{A_1,A_2} is plotted in Fig. 7 as a function of axial width of dA_1 used for integration over A_1. Figure 7 shows that an axial width of dA_1 of ~0.02 is satisfactory for F_{A_1,A_2} to converge to five significant digits, which is considered to be of acceptable accuracy.

View Factor from Cone to End Disk

Numerical results for the view factor from the lateral surface of cone to the end disk is presented for a conical enclosure inside which

Table 2 View factor results for the sample enclosure[a]

	A	B	C	D	E	
Area	28.2743	113.0973	35.1241	9.4248	28.2743	Sum
A	0.000000	0.828426	0.103574	0.019788	0.048211	0.999999
B	0.207107	0.532802	0.103683	0.029572	0.126836	1.000000
C	0.083376	0.333853	0.192221	0.095297	0.295252	0.999999
D	0.056986	0.354869	0.355153	0.000000	0.232992	0.999999
E	0.048211	0.507345	0.366780	0.077664	0.000000	0.999999

[a]Entries in the table are the view factors.

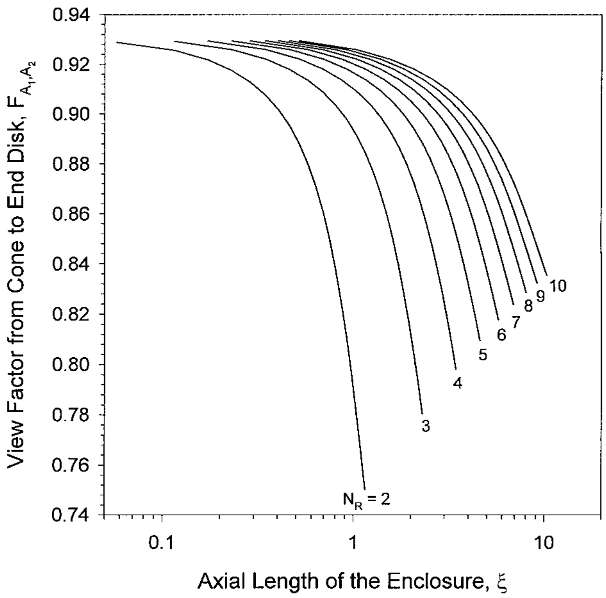

Fig. 8 Variation of view factor from cone to end disk with enclosure length for cone angle $\beta = 60$ deg and for various end disk radii.

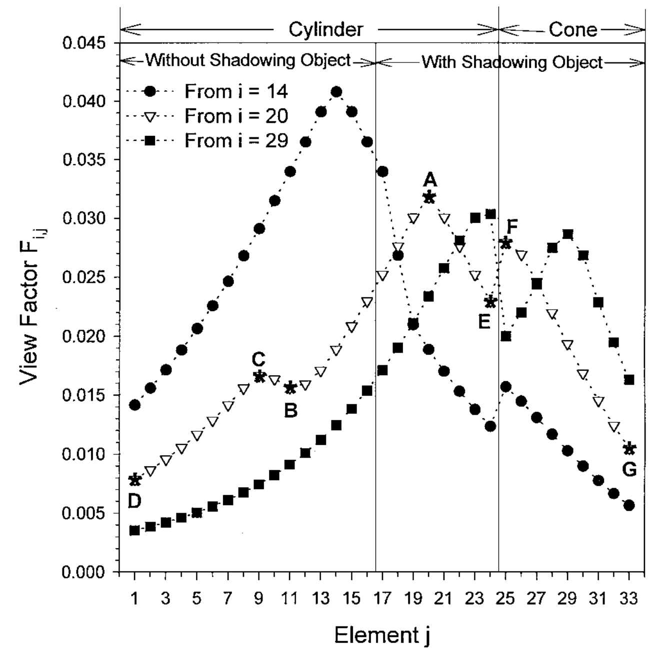

Fig. 9 View factors from three typical elements to all other elements of the sample enclosure, including shadowing effect.

a coaxial cylinder is present. To obtain the results in the most usable form, the results are described in terms of dimensions normalized with respect to the inside cylinder radius. In Fig. 8 the view factor from the lateral surface to the end disk F_{A_1,A_2} is plotted for a range of dimensionless disk radii N_R for a cone angle of 60 deg, as a function of nondimensional axial length ξ of the enclosure. The conical enclosure can have a maximum axial length of $L = (N_R - 1)/\tan\beta$ as a limiting case, when the lateral surface of the cone touches the inside cylinder as shown in Fig. 4. On the other hand, when cone angle $\beta = 0$ deg, the configuration reduces to the case of two coaxial cylinders, which is another limiting case. For both limiting cases view factors from the lateral surface of the enclosure to the end disk can be obtained by using view factor expressions available for concentric cylinder configuration and view factor algebra.[15] For the first limiting case when the lateral surface of the cone touches the inside cylinder, $F_{A_2,D}$ and $F_{A_2,C}$ (Fig. 4) can be obtained by using expressions for view factors for the concentric cylinder configuration. By view factor algebra $F_{A_2,A_1} = F_{A_2,D} + F_{A_2,C}$, and by reciprocity F_{A_1,A_2} can be calculated.

The view factors obtained by evaluating F_{dA_1,A_2} by Eq. (14) and integrating numerically by Simpson's one-third rule over the lateral surface of the cone for both these limiting cases are compared in Table 1 with those obtained by the preceding procedure.[15] When a suitable axial width of dA_1 is adapted for the numerical integration, as it can be seen from Table 1, the view factors can be calculated accurately up to six significant digits.

Application to a Sample Enclosure

To demonstrate further the usefulness of the method indicated in this paper, we present below a view factor analysis of a sample enclosure shown in Fig. 1, with dimensions $L_1/R_1 = 6$, $L_2/R_1 = 2$, $L_3/R_1 = 4$, $R_2/R_1 = 3$, and $R_3/R_1 = 2$. The assumption is made that an axial width of elements on the enclosure $\sim$0.25 is required for the thermal analysis, which is the requirement for most spacecraft applications because of the presence of thermal diffusion. This element size requirement enables the enclosure to have a total of 33 elements, of which 24 elements (1–24) are on the cylindrical portion, and the remaining 9 elements (25–33) are on the conical portion of the enclosure. View factors between elements on the enclosure (1–33) were calculated by the method just presented. View factors for the two end disks and the shadowing element (the inside cylinder) were calculated using expressions available in the literature and view factor algebra.[15]

View factors from three typical elements 14, 20, and 29 (14 on cylindrical portion where there is no shadowing object inside, 20 on cylindrical portion where the shadowing object is present, and 29 on conical portion of the enclosure) to all other elements on the enclosure are plotted in Fig. 9. View factors from element 20 to the elements to the left gradually decrease until element 11 is reached (curve A-B). However, elements 9 and 10 can see more of element 20 as they lie in region II with respect to element 20 discussed earlier, and hence have larger view factors (curve B-C). Elements 1–8 lie in region III with respect to element 20 where there is no shadowing of element 20 because of the presence of the inside cylinder, and hence, a few of these elements have larger view factors than some of the elements that are nearer to element 20 (curve C-D). Further, the orientation of the conical portion of the enclosure enables the elements on this portion to have larger view factors to node 20 than the elements, which are nearer to element 20 on the cylindrical portion of the enclosure (curve F-G). Similar explanations hold good for other results shown in the figure. The results are now presented in the form of a view factor matrix along with the view factor sums for each row of the matrix in Table 2, identifying surface A-E as comprising the enclosure (Fig. 1). Each surface A-E must satisfy the sum rule. The maximum deviation from the sum rule as seen from the table is 2×10^{-6} %. Note that all of the view factors have been calculated independently. Thus the view factors may be calculated with an error less than one digit in the sixth decimal place. The necessary computing time on a Pentium 233 MHz computer for obtaining these results was about 1 h.

Conclusion

It is clear that evaluating view factors using contour integration for the sample enclosure with the integration over finite lengths done by Simpson's one-third rule yields very accurate results with a maximum deviation of a view factor sums of the order of 2×10^{-6} % and with an accuracy of view factors up to six significant digits. The analytical expression and graphs presented for the view factors in a conical enclosure inside which a coaxial cylinder is present are significant contributions to the literature. The method indicated could be applied to any enclosure inside which shadowing objects are present, when all of the bodies are axisymmetric bodies of revolution, which are common in space applications. If the shadowing objects are not axisymmetric, the same method can be used with one more numerical integration to be carried out in the circumferential direction.

Acknowledgment

The authors thank one of the reviewers for pointing out an error and also for suggesting changes that have improved the paper significantly.

References

[1]Pisacane, V. L., and Moore, R. C. (eds.), *Fundamentals of Space Systems*, Johns Hopkins Univ./Applied Physics Lab. Series in Science and Engineering, Oxford Univ. Press, Oxford, 1994, p. 445.

[2]Ambirajan, A., and Venkateshan, S. P., "Accurate Determination of Diffuse View Factors Between Planar Surfaces," *International Journal of Heat and Mass Transfer*, Vol. 36, No. 8, 1993, pp. 2203–2208.

[3]Siegel, R., and Howell, J. R., *Thermal Radiation Heat Transfer*, 3rd ed., Taylor and Francis, Washington, DC, 1972, Appendices B and C.

[4]Usiskin, C. M., and Siegel, R., "Thermal Radiation from a Cylindrical Enclosure with Specified Wall Heat Flux," *Journal of Heat Transfer*, Vol. 82, No. 4, 1960, pp. 369–374.

[5]Sparrow, E. M., Albers, L. U., and Eckert, E. R. G., "Thermal Radiation Characteristics of Cylindrical Enclosures," *Journal of Heat Transfer*, Vol. 84, No. 1, 1962, pp. 73–81.

[6]Sparrow, E. M., and Jonsson, V. K., "Radiant Emission Characteristics of Diffuse Conical Cavities," *Journal of the Optical Society of America*, Vol. 53, No. 7, 1963, pp. 816–821.

[7]Hamilton, D. C., and Morgan, W. R., "Radiation-Interchange Configuration Factors," NASA TN 2836, Dec. 1952.

[8]Leuenberg, R. H., and Person, R. A., "Compilation of Radiation Shape Factors for Cylindrical Assemblies," American Society of Mechanical Engineers, Paper 56-A-144, Nov. 1956.

[9]Srinivasan, R., and White, A., C., "Analytical Expression for a Concentric-Cylinder Radiation View Factor," *Journal of Thermophysics and Heat Transfer*, Vol. 10, No. 3, 1996, pp. 534–536.

[10]Sparrow, E. M., Miller, G. B., and Jonsson, V. K., "Radiating Effectiveness of Annular-Finned Space Radiators, Including Mutual Irradiation Between Radiator Elements," *Journal of the Aerospace Sciences*, Vol. 29, No. 11, 1962, pp. 1291–1299.

[11]Ramesh, N., and Venkateshan, S. P., "Optimum Finned Tubular Space Radiator," *Heat Transfer Engineering*, Vol. 18, No. 4, 1997, pp. 69–87.

[12]Sunil Kumar, S., and Venkateshan, S. P., "Optimized Tubular Radiator with Annular Fins on a Non-Isothermal Base," *International Journal of Heat and Fluid Flow*, Vol. 15, No. 5, 1994, pp. 399–409.

[13]Meng, X. Y., and Zhang, C. M., "Calculation of Radiation Shape Factors Between Many Bodies Including the Inner Walls of an Irregularly Shaped Chamber," *Proceedings of the Seventh International Conference Held in Stanford*, Vol. 7, Pt. 1, Pineridge Press, Swansea, Wales, U.K., 1991, pp. 797–807.

[14]Sparrow, E. M., "A New and Simpler Formulation of Radiative Angle Factors," American Society of Mechanical Engineers, Paper 62-HT-17, 1962; also *Journal of Heat Transfer*, Vol. 85, No. 2, 1963, pp. 81–88.

[15]Sparrow, E. M., and Cess, R. D., *Radiation Heat Transfer*, rev. ed., Brooks/Cole Publishing Co., Belmont, CA, 1970, Appendix A.